Nanoelectronics

DOI: 10.1002/anie.200705109

Light-Emitting Diodes with Semiconductor Nanocrystals

*Andrey L. Rogach, Nikolai Gaponik, John M. Lupton, Cristina Bertoni, Diego E. Gallardo, Steve Dunn, Nello Li Pira, Marzia Paderi, Piermario Repetto, Sergei G. Romanov, Colm O'Dwyer, Clivia M. Sotomayor Torres, and Alexander Eychmüller**

Keywords:
light-emitting diodes · nanocrytals · nanoelectronics · quantum dots · semiconductors

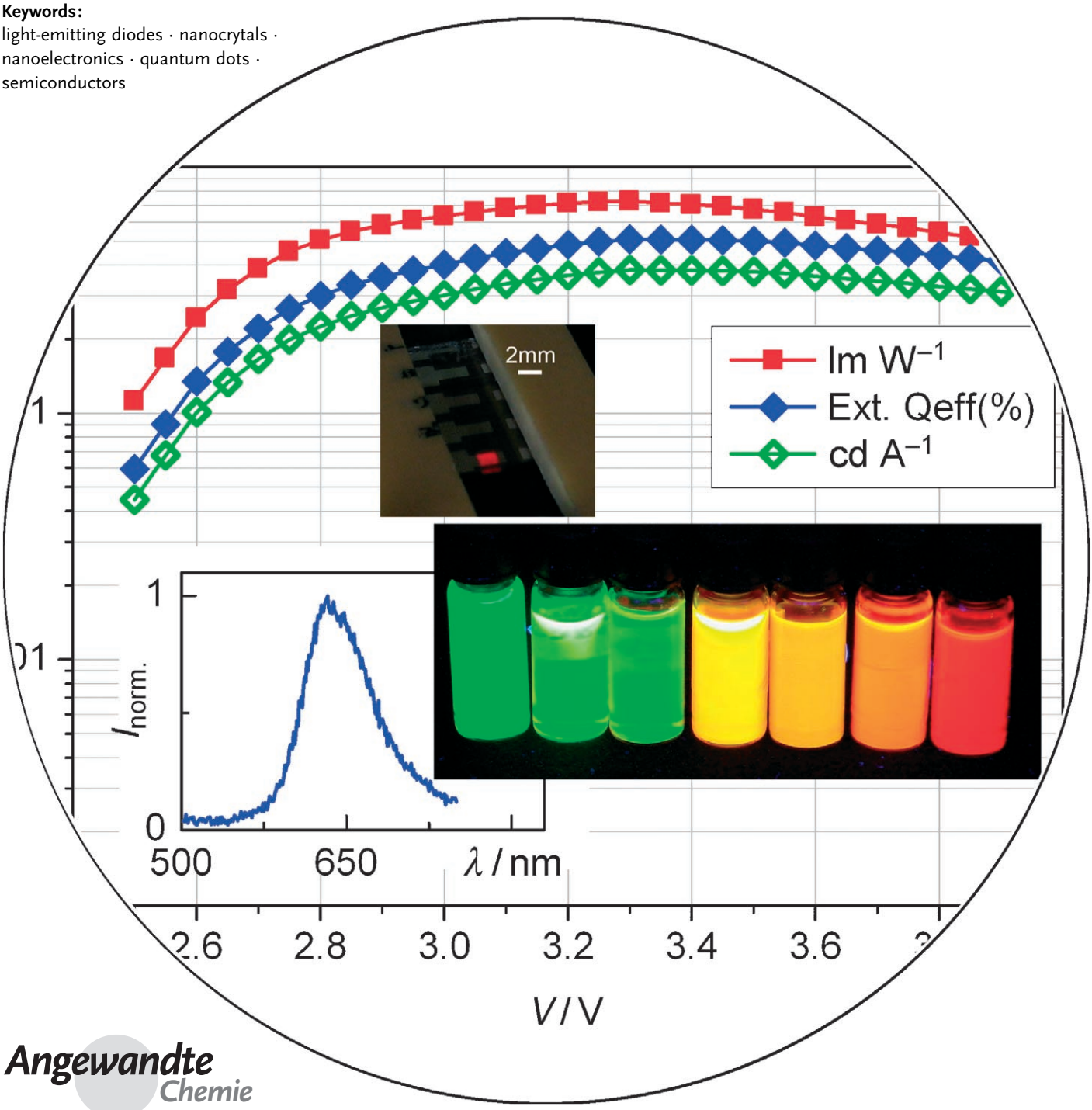

Colloidal semiconductor nanocrystals are promising luminophores for creating a new generation of electroluminescence devices. Research on semiconductor nanocrystal based light-emitting diodes (LEDs) has made remarkable advances in just one decade: the external quantum efficiency has improved by over two orders of magnitude and highly saturated color emission is now the norm. Although the device efficiencies are still more than an order of magnitude lower than those of the purely organic LEDs there are potential advantages associated with nanocrystal-based devices, such as a spectrally pure emission color, which will certainly merit future research. Further developments of nanocrystal-based LEDs will be improving material stability, understanding and controlling chemical and physical phenomena at the interfaces, and optimizing charge injection and charge transport.

From the Contents

1. Introduction

The advantages of the rapidly developing organic light-emitting diode (OLED) technology[1] can be combined with attractive properties of semiconductor nanocrystals (NCs).[2] The optical properties of this class of lumophores are determined by the quantum confinement effect,[3] so that their emission color (Figure 1) and the electron affinity can be controlled not only by the material choice but also by the size which can be tailored during the synthetic procedure.

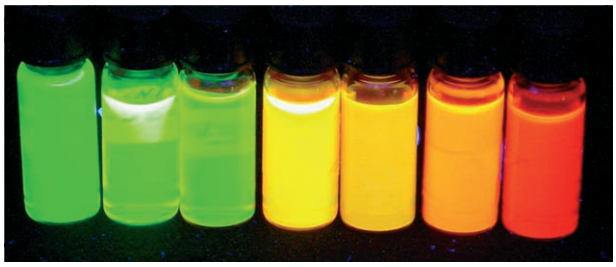

Figure 1. Size-dependent photoluminescence of CdTe nanocrystals synthesized in water (2–5 nm size range, the smallest particles emit green, the largest red, the quantum efficiency is up to 60%).

A typical semiconductor nanocrystal, which can also be thought of as a colloidal quantum dot, consists of an inorganic core, which is comparable to or smaller in size than the Bohr exciton diameter of the corresponding bulk material, surrounded ("passivated") by an organic shell of ligands.[2] State-of-the-art syntheses, which can be carried out either in organic solvents[4] or in water,[5] provide different II–VI, III–V, and IV–VI nanocrystals with variable size and a narrow size distribution leading to narrow emission spectra (25–35 nm full width at half maximum (FWHM) in solution) for which the emission maximum is tunable from the UV to the near-infrared spectral region.[6] We refer interested readers to some recent[7–9] and less-recent[10,11] reviews on the synthesis of semiconductor nanocrystals. Proper surface passivation leads to improved chemical stability and high photoluminescence (PL) quantum efficiencies of $>50\%$ for so-called Type I core–shell[12,13] nanocrystals, such as CdSe/ZnS, where the large band-gap semiconductor (e.g. ZnS) overgrows the core material epitaxially (CdSe) and the band edges of the core material lie inside the band gap of the outer material. The variety of surface chemistries possible with nanoparticles enables their simple processing from different solvents and facilitates their incorporation into different organic matrices.[14] However, the conduction properties of nanocrystal-only films are poor,[15–17] and it is difficult to achieve an electrical contact to single nanocrystals because of their small size. However, in general, their properties make nanocrystals attractive materials for fabrication of hybrid semiconductor-nanocrystal–organic LEDs with a highly saturated emission

[*] Dr. N. Gaponik, Prof. A. Eychmüller
Physical Chemistry, TU Dresden
Bergstrasse 66b, 01062 Dresden (Germany)
Fax: (+49) 351-463-37164
E-mail: alexander.eychmueller@chemie.tu-dresden.de

Dr. A. L. Rogach
Photonics & Optoelectronics Group, Physics Department and Center for NanoScience (CeNS), Ludwig-Maximilians-Universität München, Amalienstrasse 54, 80799 Munich (Germany)

Dr. C. Bertoni, Dr. D. E. Gallardo, Dr. S. Dunn
Nanotechnology Group, SIMS, Cranfield University
Beds, MK43 0AL (UK)

Dr. N. Li Pira, Dr. M. Paderi, Dr. P. Repetto
Nanomanufacturing—Technologies Division
Centro Ricerche Fiat
Strada Torino 50, 10043 Orbassano (TO) (Italy)

Dr. S. G. Romanov, Dr. C. O'Dwyer, Prof. C. M. Sotomayor Torres
Tyndall National Institute, University College Cork
Lee Maltings, Cork (Ireland)

Prof. J. M. Lupton
Physics Department, University of Utah, Salt Lake City, Utah 84112 (USA)

color. This property is of importance for the development of full color large-area flat-screen displays.

This Review provides an overview of LEDs based on semiconductor nanoparticles operating in the visible spectral region, typically with an organic component, and is divided into two parts which describe the devices processed from organic and from aqueous solutions. The organic component of the hybrid LEDs is either (and mainly) a conjugated polymer, such as poly(*para*-phenylenevinylene) (PPV), a non-conjugated polymer, such as polyvinylcarbazole (PVK), or consists of small organic molecules, such as aluminum-tris-(8-hydroxyquinoline) (Alq_3). Nanocrystal-based LEDs emitting in the near-infrared spectral range have been reviewed in a previous publication.[6] In addition, we review some recent progress in understanding the influence the unique morphology of nanoparticle films and nanoparticle–molecule blend films has on the performance of thin-film devices. This feature is of particular relevance for LEDs in which high fields act on the layers and electrodes and electrode decomposition effects can be significant. This decomposition leads to a surprisingly high mobility of elemental contaminants in the comparatively porous hybrid layers, an issue that clearly needs to be addressed when designing stable high-power nanoparticle-based light emitters.

2. Nanocrystal-Based Devices Processed from Organic Solvents

The first paper on hybrid nanocrystal/polymer LEDs appeared in 1994.[18] Alivisatos and co-workers reported a bilayer device comprising a thin layer of CdSe nanocrystals deposited on a conducting support and a 100 nm thick layer of a soluble PPV derivative. The structure was sandwiched between an ITO-coated glass (anode) and an Mg/Ag electrode (cathode). The device, which had a hole-transporting PPV layer close to the ITO, and in which electrons were injected into a layer of nanocrystals, and holes were injected into a layer of polymer (forward bias), exhibited an emission characteristic of the CdSe nanocrystals at an operating voltage of only 4 V. The electroluminescence (EL) band could be tuned from yellow to red by changing the nanocrystal size. The current–voltage (*I–V*) characteristics were determined by electron injection at the Mg/CdSe nanocrystal interface, which constituted the current-limiting mechanism. The recombination zone most likely lay within the CdSe nanocrystal layer close to the CdSe/PPV interface. At higher voltages, green emission from the PPV layer predominated, giving rise to a voltage-dependent color of this device (Figure 2).

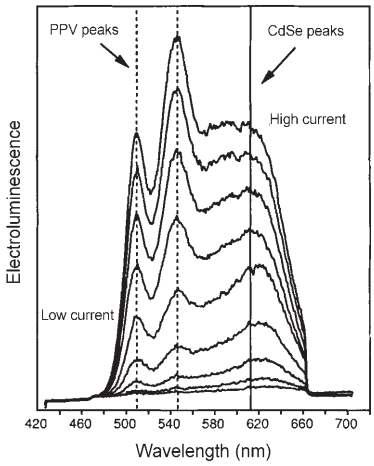

Figure 2. Voltage-dependent color of a CdSe nanocrystal/PPV device. Reprinted from [18], Copyright 1994, with permission from Nature Publishing Group.

A subsequent paper from two groups at MIT[19] reported a single-layer device where CdSe nanocrystals were homogeneously distributed within a polymer layer (70–120 nm thick) of PVK as a hole-conducting component that additionally contained an oxadiazole derivative (2-(4-biphenyl)-5-(4-*tert*-butylphenyl)-1,3,4-oxadiazol (butyl-PBD)) as an electron-transporting molecular species. The resulting volume fraction of CdSe nanocrystals in a film sandwiched between ITO and Al electrodes was 5–10 %, a value below the percolation threshold for charge transport to occur between the nanocrystals. The photoluminescence and electroluminescence spectra of the devices were reasonably narrow (< 40 nm FWHM), nearly identical, and the emission maximum could be tuned from 530 to 650 nm by varying the nanocrystal size. The current–voltage traces showed near inversion symmetry, and the electroluminescence in reverse bias showed no change in the spectral line shape compared to that at the forward bias, indicating that nanoparticles were not directly involved in the carrier transport. Both the injection of electrons and holes by tunneling through the organic ligands were considered as excitation mechanisms of the nanocrystals as well as Förster energy transfer from excitations formed in the organic host.

While the external quantum efficiencies of these first, unoptimized devices were low, 0.001–001 %[18] and 0.0005 %[19] these studies showed in principal a possibility of generating a spectrally pure electroluminescence from semiconductor nanoparticles in hybrid devices. In this case the electroluminescence can be tuned by changing the physical size of the nanocrystal rather than having to change the actual

Alexander Eychmüller studied physics at the University of Göttingen. In 1987 he obtained his Ph.D. working on proton-transfer reactions under the supervision of Dr. K.-H. Grellmann and Prof. A. Weller at the Max-Planck-Institute for Biophysical Chemistry. After a postdoc at UCLA with Prof. M. A. El-Sayed on gas-phase metal clusters he joined the group of Prof. A. Henglein at the Hahn-Meitner-Institute in Berlin where he became involved in the research on semiconductor quantum dots. He moved to the University of Hamburg with Prof. H. Weller and studied photophysical and structural properties of semiconductor nanocrystals, completing his Habilitation in 1999. Since 2005 he has been Professor of Physical Chemistry and Electrochemistry at the TU Dresden.

chemistry of the material as is often the case for organic chromophores. Subsequently the same groups reported bilayer devices based on core–shell nanocrystals.[20,21] The devices reported in Ref. [20] consisting of a spin-deposited layer of PPV on an ITO support and a spin-deposited layer of core–shell CdSe/CdS nanocrystals adjacent to a Mg/Ag electrode showed significant improvements over the core-only CdSe-based devices, namely a factor of 20 increase in quantum efficiency and a factor of 100 in lifetime. These devices could be tuned to emit from the green to the red with external quantum efficiencies of up to 0.22% at brightnesses of 600 cd m^{-2} and current densities of 1 A cm^{-2}, with operating voltages of 4 V and lifetimes under direct current of hundreds of hours. Similar characteristics were reported in Ref. [21] on a comparable bilayer device made of bare CdSe or core–shell CdSe/ZnS nanocrystals spin-cast from toluene solution on a PPV layer, which in turn was built up from aqueous solution by the layer-by-layer deposition technique in combination with polymethacrylic acid (PMA). The PPV/PMA film served as a hole-transport layer and reduced the flow of electrons, thereby moving the electron–hole recombination zone away from the anode. The neat film of nanocrystals was the electron-transport layer which also served as the exciton recombination zone. Figure 3 shows size-dependent electro-

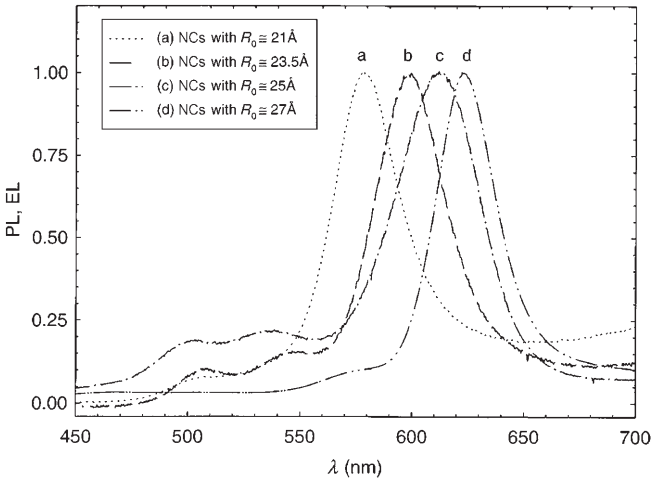

Figure 3. Size-dependent color of a CdSe nanocrystal/PPV device. PL: photoluminescence, EL: electroluminescence. Reprinted from [21], Copyright 1998, with permission from the American Institute of Physics.

luminescence spectra of these devices employing bare CdSe nanocrystals and demonstrating a color tunability over a range of 80 nm. Evidently, there is still a considerable amount of PPV emission. This emission is due to the fact that direct recombination can also occur in the PPV layer.

Further examples of hybrid nanocrystal/polymer LEDs emitting in the visible include single-layer devices constituting ZnS nanocrystals synthesized in situ in a PMA–polystyrene (PS) matrix doped with tetraphenylbenzidine as a hole-transport material;[22] multilayer LEDs containing manganese-doped ZnS[23] or isolated CdSe/ZnS nanocrystals covered by various organic ligands;[24] and CdSe/ZnS-based LEDs, where the nanocrystal layers of different thicknesses were deposited on an ITO substrate coated with poly(3,4-ethylenedioxythiophene) doped with polystyrene sulfonated acid (PEDOT:PSS) upon which various metal electrodes (Ba, Al, or Au) were subsequently deposited.[25] The latter configuration has been improved by the same group using a hole-conducting layer of PVK and an electron-conducting layer of 1,3,4-tris(2-*N*-phenylbenzimidazol)-benzene (TPBI).[26] Elongated CdSe/CdS nanocrystals (nanorods) were embedded between these layers in an oriented fashion, providing LEDs emitting polarized light.[26] All-inorganic multicolor LEDs based on CdSe/ZnS nanocrystal mono- or bilayers built into a p-n junction formed from GaN charge-injection layers by energetic neutral atom beam lithography have been realized.[27] It was also shown that non-radiative energy transfer from electrically driven InGaN/GaN quantum wells to semiconductor nanocrystals results in an efficient color conversion.[28] The very recent development of the hybrid nanocrystal/polymer multilayer LED configurations are based on a monolayer of colloidal CdSe/CdS nanocrystals deposited by spin-coating on top of thermally polymerized solvent-resistant hole-transport layers where the use of multiple spin-on organic layers improves the external quantum efficiency of the LEDs to 0.8% at a brightness of 100 cd m^{-2}.[29] In situ thermal annealing of the nanocrystal layer improved the film morphology, resulting in a better electrical injection from the organic layers to the nanocrystals and giving in a three to fourfold enhancement of the device efficiency, with emission exclusively from the nanocrystals.[30] The issue of long-term stability of brightly emitting nanocrystal-based LEDs emitting in pure and saturated spectral colors has been addressed in Ref. [31]

Trilayer hybrid nanocrystal/OLEDs with a single monolayer of CdSe/ZnS nanocrystals sandwiched between two organic thin films have been introduced by two groups at MIT.[32,33] In these devices, the luminescence function of the nanoparticles was isolated from their participation in charge conduction so that the organic layers transported charge carriers to the vicinity of the nanocrystal monolayer from which the narrow-band electroluminescence originated. This set up differs from most of the previously reported concepts in which the nanocrystals had the dual function of both transporting electrons and serving as the emissive layer. An elegant phase-separation approach utilizes self-segregation of trioctylphosphine oxide (TOPO) capped nanocrystals from the aromatic molecules of the hole-transporting material *N*,*N*′-diphenyl-*N*,*N*′-bis(3-methylphenyl)-(1,1′-biphenyl)-4,4′-diamine (TPD). Spin-coating this mixture in chloroform onto ITO substrates, led to the formation of a complete single nanocrystal monolayer on top of a 35 nm thick TPD film. The final device was formed by thermal evaporation of a 10 nm thick layer of 3-(4-biphenyl)-4-phenyl-5-tert-butylphenyl-1,2,4-triazole (TAZ), followed by a 40 nm thick layer of Alq_3 and a Mg/Ag electrode. The function of TAZ was to block the holes and confine the excitons, leading to a narrower emission band with lower contributions from the TPD and Alq_3 electroluminescence than in similar devices without the TAZ layer (Figure 4). The external quantum efficiency of the device without TAZ was approximately 50%

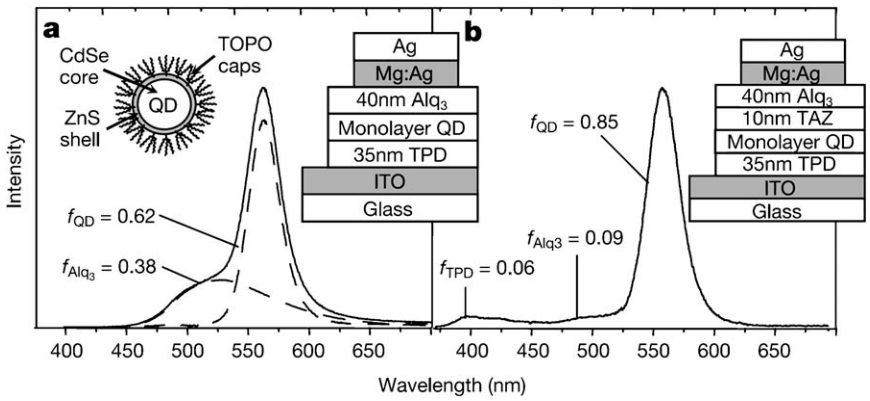

Figure 4. Electroluminescence spectra and schematic structures of two kinds of trilayer hybrid nanocrystal/organic molecule LEDs (with and without TAZ layer). Reprinted from [32], Copyright 2002, with permission from Nature Publishing Group.

higher than in the presence of TAZ and exceeded 0.4% for a broad range of luminances. At 125 mA cm^{-2}, the brightness of the three-layer device was 2000 cd m^{-2} (i.e. 1.6 cd A^{-1}), which is a 25-fold improvement over the best reported nanocrystal-based LEDs at that time.[20]

Although these devices exhibited a much faster response time than previous systems, further studies are required to establish whether the exceptionally high switching speeds observed in all-organic LEDs can be matched by hybrid-device structures. High switching speeds would be interesting for implementing wavelength division multiplexing (WDM) in optical communications, in which plastic-based LEDs are particularly interesting owing to the possibility having the emitter and detector directly incorporated onto the bent surface of an optical fiber. The narrow band emission of nanocrystals makes the color selectivity required for WDM particularly feasible. In Ref. [33], additional studies on the devices utilizing CdSe nanoparticles with variable ZnS shell thickness have shown that Förster energy transfer of excitons from organic materials to the nanocrystals dominates the electroluminescence process, rather than direct charge injection into nanocrystals. For the CdSe/ZnS-based devices with thicker ZnS shells, external quantum efficiencies of 1.1% were achieved.

A final interesting point in the monolayer-device structure is the possibility of generating very high excitation densities at a well-defined position. This ability could prove useful for achieving the long sought-after goal of electrically pumped lasing in an organic semiconductor. Color-saturated green-emitting LEDs built by the same concept, with core–shell alloyed $Cd_xZn_{1-x}Se/Cd_yZn_{1-y}S$ nanocrystals as an active monolayer have been demonstrated.[34] After these successful developments, trilayer hybrid nanocrystal/polymer devices were reported, comprising a film of CdSe/ZnS nanocrystals a few monolayers thick sandwiched between films of PVK and butyl-PBD.[35] All the layers were deposited by the spin-coating technique from dissimilar solvents (organic or water). These devices showed 20-times the external quantum efficiency (0.2%) and less than half the threshold voltage of a single-layer device based on the PVK/nanocrystal/PBD blend. These improvements upon going from a blend to a trilayer structure were attributed to more balanced carrier conduction and to enhanced recombination in the nanocrystal layer.

In addition to nanoparticle-based LEDs with monochromatic emission, white-light-emitting devices have also attracted much interest,[36] both for their potential application in large area displays and in the lighting industry. To achieve white emission, the three primary colors, or two complementary colors, must be combined. White hybrid organic–inorganic light-emitting devices have been fabricated by using stable red-emitting CdSe/ZnS core–shell nanocrystals covered with a TOPO organic ligand. The device-active structure consists of a host–guest system with a blue-emitting poly[(9,9-dihexyloxyfluoren-2,7-diyl)-alt-co-(2-methoxy-5-{2-ethylhexyloxy}phenylen-1,4-diyl)] (PFH-MEH) polymer doped with red-emitting nanocrystals and a green-emitting metal chelate complex Alq_3, which improves the electron injection and transfer properties.[37] A fairly pure white OLED with Commission Internationale de l'Eclairage (CIE) coordinates of (0.30, 0.33) is fabricated by accurate control of the Förster energy transfer and charge-transfer mechanisms between the different components. Maximum external quantum efficiencies up to 0.24% at 1 mA cm^{-2} and 11 V in air atmosphere are reported, showing that hybrid LEDs can be a promising route towards more stable and efficient light-emitting devices for lighting applications.

In another recent publication,[38] LEDs with a broad spectral emission generated by electroluminescence from a mixed-monolayer of red, green, and blue emitting nanocrystals in a hybrid organic–inorganic structure have been realized. Independent processing of the organic charge-transport layers and the nanocrystal luminescent layer allowed for precise tuning of the emission spectrum without changing the device structure. The tuning is carried out simply by changing the ratio of different color nanocrystals in the active layer. This tuning resulted in white nanocrystal-based LEDs that exhibited external quantum efficiencies of 0.36% and emitted at CIE coordinates of (0.35, 0.41).

In a recent publication we have shown that surface-passivated nanoparticles, such as CdSe/ZnS core–shell nanocrystals could be used to fabricate white-light emissive LEDs by combining the green to red emissions of the nanocrystals with blue emission from organic molecules.[39] As a blue–green emitting organic material 2,7-Bis[2-(4-diphenylaminophenyl)-1,3,4-oxadiazole-5-yl]-9,9-dihexylfluorene (BADF) was chosen because of its relatively low turn-on voltage for electroluminescence and high photoluminescence quantum efficiency of 86%.[40] Two OLED architectures, A and B (Figure 5), were studied. For Device A, a hole-injection layer, poly(3,4-ethylenedioxythiophene) doped with polystyrene sulfonated acid (PEDOT:PSS), was spin-coated onto the ITO prior to the deposition of the organic materials. The blend solution was spin-coated to make 100 nm thick films. Calcium (40 nm) and aluminum (100 nm) circular top electrodes, 2 mm diameter, were then thermally evaporated, sequentially, and at a pressure of about 10^{-6} mbar. In the case of

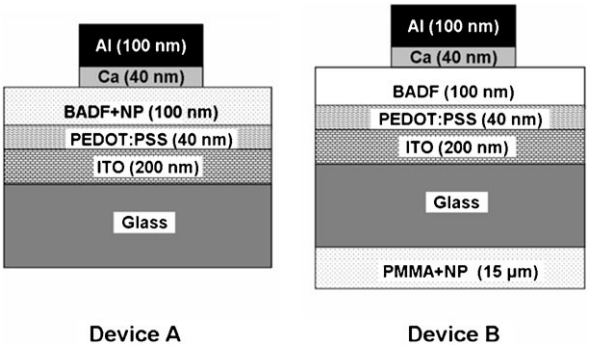

Figure 5. Schematic device architectures of two nanoparticle (NP) based OLEDs. Reprinted from Ref. [39], copyright 2007, with permission from IOPP.

Device B, a color-conversion layer was formed on the uncoated (non-ITO) side of the substrate. Poly(methyl methacrylate) (PMMA) was added to the nanocrystal solution (33 $g\,L^{-1}$) and the resulting mixture was dropped onto the glass surface and dried in an atmosphere saturated with chloroform vapor (to retard the vaporization of the solvent). The planar density of the solution, 50 $\mu L\,cm^{-2}$, resulted in a 15 μm thick layer. After this layer was fully dried, the ITO side of the substrate was cleaned by rubbing the surface using acetone-soaked cotton balls. PEDOT:PSS was then spin-coated and the fabrication method for Device A was followed, but using BADF instead of the BADF:nanoparticle blend

Figure 6 shows the electroluminescence emission of Device A (ITO/PEDOT:PSS/BADF:nanoparticle-blend/Ca/Al). The spectrum of the pure BADF device is also given for comparison. The red emission from the CdSe/ZnS nanoparticles is clearly evident, together with the blue–green emission from BADF. The electroluminescence from the pure BADF device showed a vibronic spectrum with peak positions at 459, 487, 521, and 557 nm. In the BADF:nanoparticle system, the photoluminescence emission spectrum of BADF and the absorption spectrum of CdSe/ZnS overlap satisfying the necessary condition for Förster energy transfer, so that the nanoparticles can be excited by both charge transfer and energy transfer from the organic dye.[41] An interesting feature in Figure 6 is the decrease in the green emission (electroluminescence peaks at 521 and 557 nm) and the increase in the blue emission (459 nm) of the blended-layer devices compared to the pure BADF OLED. This green emission originates from oxidative keto-type defects which form fluorenones, which are generally populated by electron trapping in electroluminescent devices. The nanocrystals serve as lower energy electron traps and therefore reduce the green emission arising from recombination on the fluorenones, enhancing the color purity.

Figure 7, top shows the CIE 1931 color coordinates of the BADF:nanoparticle-blend Device A, for which the electroluminescence spectrum was shown in Figure 6. The color coordinate moved to the blue region as the bias increased, and

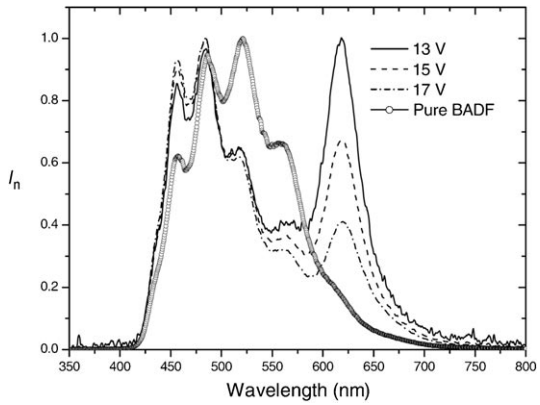

Figure 6. Electroluminescence spectra of the Device A (see Figure 5) with blended BADF layer. The electroluminescence for a pure BADF OLED is shown for reference; I_n: normalized intensity. Reprinted from Ref. [39], copyright 2007, with permission from IOPP.

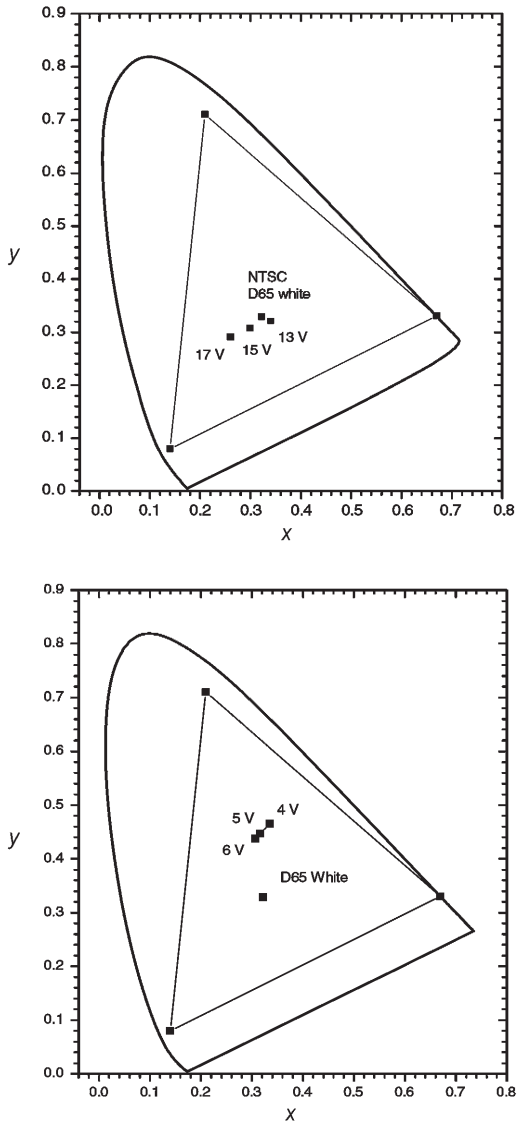

Figure 7. Top: CIE color coordinate of Device A (see Figure 5) at various applied voltages. The coordinate of NTSCD65 white was included for comparison. Below: the same plot for Device B (see Figure 5). Reprinted from Ref. [39], copyright 2007, with permission from IOPP.

as the red emission, evident in Figure 6, decreased. The CIE color coordinates were (0.340, 0.321), (0.299, 0.308), and (0.260, 0.291) at 13, 15, and 17 V, respectively. The blended-layer OLED gave good white emission. However, the device efficiency was more than an order of magnitude less than that of the pure BADF device. This result means more than 90% of the emission ability of the blue–green emitter was effectively lost. The variation in the relative intensity of nanoparticle emission with the applied bias is a further problem, as the emission color will change with the intensity. A possible solution to this is to separate the organic semiconductors and nanoparticles, this was achieved in Device B (nanocrystal/glass/anode/organic-material/cathode; Figure 5) with the nanocrystal layer on the backside of the substrate. The CIE color coordinates of the Device B structures were (0.335, 0.465), (0.315, 0.447), and (0.307, 0.438) at 4, 5, and 6 V (Figure 7, bottom). The purity of the white emission was poor, with a color on the green–yellow boundary of white. This color was a result of the relatively low red emission from the nanoparticles. The maximum external quantum efficiency of the BADF device with the color-conversion layer was 0.41% at 8.6 $mA\,cm^{-2}$ whereas that of the pure BADF device was 0.25% at 32 $mA\,cm^{-2}$. The current and power efficiencies for Device B structures were 0.51 $Lm\,W^{-1}$ and 0.96 $cd\,A^{-1}$ (at 5.9 V and 100 $cd\,m^2$), respectively, compared to figures of 0.35 $Lm\,W^{-1}$ and 0.70 $cd\,A^{-1}$ (at 6.3 V and 100 $cd\,m^{-2}$) for the pure BADF OLED.

The increase in the efficiency of the Device B structures is intriguing. However, we are convinced that this is a real effect and not the result of device-to-device variations. In fact, a similar phenomenon has also been observed by Duggal and co-workers when a color-conversion layer consisting of organic dyes and phosphor particles was placed on the back side of the substrate.[42] Generally, a modification to the backside of the substrate (e.g. using a lens layer) is needed to achieve such an efficiency increase (the refractive indices of glass and PMMA are very similar). Duggal et al. explained the effect by the scattering of light by phosphor particles. It is possible that our PMMA:nanocrystal mixture resulted in a similar process. However, as the nanoparticles used in this system are much smaller than the wavelength of the emitted light, any scattering will probably originate from clusters of nanoparticles.

In Table 1, we summarize the most important examples of nanocrystal-based LED configurations reported in the literature.

3. Nanocrystal-Based Devices Processed from Aqueous Solution

Another interesting class of nanocrystals are those synthesized in aqueous solutions. The state of the art syntheses allow for the fabrication of efficiently emitting nanocrystals (photoluminescence quantum efficiency 30–60%), such as, ZnSe nanocrystals (UV-blue spectral region),[43] CdTe nanocrystals (visible),[5,44,45] CdHgTe and HgTe nanocrystals (NIR).[46] Water-soluble CdTe nanoparticles have been incorporated into pre-formed films of electrochemically polymerized polyaniline,[47] and polypyrrole has been electrochemically deposited from aqueous solution within the pores of drop-cast CdTe nanocrystal films.[48] Both of these device geometries led to visible-light emission at low biases of 2.5–3 V. Nanocrystals synthesized by the aqueous approach can be made charged at specific pH values because of the free functional groups on the ligand molecules (typically -COOH or -NH_2 in case of thioacids and thioamines). This feature allows processing of nanoparticles by the layer-by-layer assembly approach. This technique, which is based on alternating adsorption of oppositely charged species, was originally developed for positively and negatively charged polyelectrolyte pairs, either insulating[49] or conducting,[50] and was later extended to the assembly of polymer-linked nanocrystals.[51] The method is very general and produces large-area high-quality homogeneous films almost irrespective of the substrate or the nanocrystal materials used, along with nanometer scale control over the thickness and composition.

The first hybrid nanocrystal-based LED made by the layer-by-layer assembly was reported in Ref. [52]. It was formed by stacking 20 alternating double layers of a precursor of PPV (pre-PPV) and CdSe nanocrystals capped by thiolactic acid, and subsequent thermal conversion of pre-PPV into PPV. The device emitted white light originating mainly from recombination through nanoparticle trap sites. It had a turn-on voltage of 3.5–5 V and an external quantum efficiency

Table 1: Summary of different nanocrystal-based LED configurations.

LED architecture	External efficiency	Nanocrystal materials, emitting wavelength	Ref.
Layer-by-layer deposited alternating layers of nanocrystals and polymers	0.1–0.5%	CdTe, 540–660 nm	[55, 57]
Blended single layer of nanocrystals and polymers	0.0005%	CdSe, 530–650 nm	[19]
Bi-layer devices of separated thin films of nanocrystals and organics	0.22% 0.8%	CdSe/CdS, CdSe/ZnS, 530–650 nm	[20, 21] [29]
Tri-layer devices with a monolayer of nanocrystals sandwiched between organic layers	0.2–1.1%	CdSe/ZnS, 530-650 nm	[32, 33, 35]
Blended single layer of nanocrystals and polymers Bi-layer devices of separated thin films of nanocrystals and organics	0.24% 00.41%	CdSe/ZnS, White light CdSe/ZnS, White light	[37] [39]

of 0.0015%. The subsequent paper from the same group[53] compared single-layer CdSe nanocrystal-based devices utilizing conducting (PPV) or non-conducting (poly(allylamine hydrochloride) (PAH)) polymers and demonstrated the possibility to build up vertically structured bilayer CdSe nanocrystal/PAH–PPV/PAH LEDs. These devices showed a predominant emission either from the preferentially hole-transporting PPV or from the preferentially electron-transporting CdSe nanocrystals, depending on the polarity of the applied field and the effective position of the recombination zone. The lifetime of the PPV emission in the bilayer device was considerably extended, which may be due to the consumption of trace oxygen by CdSe nanocrystals. CdSe can bind oxygen to its surface which may prove beneficial in two ways: Firstly, nanocrystals could help reduce the level of oxygen in organic semiconductors, where oxygen is detrimental to operation, and secondly, molecular oxygen can actually lead to a dramatic enhancement in fluorescence efficiency from the nanoparticles as a result of more efficient neutralization following an undesired photochemical charging event.[54]

Electroluminescence of different colors (from green to red; Figure 8) was obtained from layer-by-layer assembled

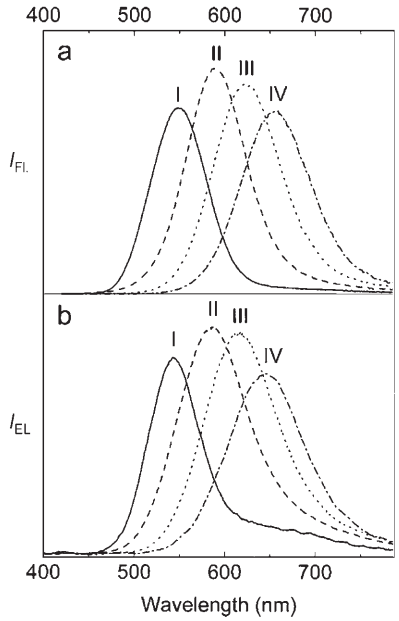

Figure 8. a) Fluorescence spectra of CdTe nanocrystals aqueous solutions excited at 400 nm; b) Electroluminescence spectra of corresponding CdTe/PDDA films. Reprinted from Ref. [55], copyright 2000, with permission from the American Institute of Physics.

LEDs based on thioglycolic acid capped CdTe nanocrystals of different sizes and poly(diallyldimethylammonium chloride) (PDDA).[55] In spite of the use of an insulating polymer, external quantum efficiencies of 0.1% were achieved. Light emission was observed at current densities of 10 mA cm^{-2} and at exceptionally low onset voltages of 2.5–3.5 V (i.e. only just above the band gap of the CdTe nanocrystals). The electroluminescence onset showed a dependence on the thickness of the film, indicating field-dependent current injection. The internal charge transport in these devices can be considered as a hopping transport between nanocrystals which act as an electron-transporting material; the transport is driven by the external electric field. The electroluminescence of bilayer devices, in which each layer consisted of 20 alternating double layers of CdTe nanocrystals, with a bimodal size distribution, and PDDA, showed emission from the nanoparticles close to the ITO electrode. Layer-by-layer assembled LEDs based on water-soluble CdTe nanocrystals and PPV were also reported.[56]

Recently, results pertaining the development of a red-emitting electroluminescent device based on thiol-capped CdTe nanocrystals in combination with PDDA has been reported.[57] The results show that the quality and uniformity of the emissive multilayer were crucial to achieve better efficiencies while the electrical characterization proves that current and electroluminescence are electric-field dependent. From the analysis of the device cross section it was estimated that each PDDA/CdTe bilayer is around 3 nm thick. This value is in agreement with the mean size of the CdTe nanocrystals used, as derived from their absorption spectra. A number of samples were produced consisting of 30, 40, and 50 bilayers. The current–voltage characteristics and the device light output were measured under normal laboratory conditions, that is, devices were not sealed or packaged. Figure 9 shows current–voltage characteristics for several devices made of 30, 40, and 50 bilayers. The curves show a clear correlation between voltage and the number of layers. All the

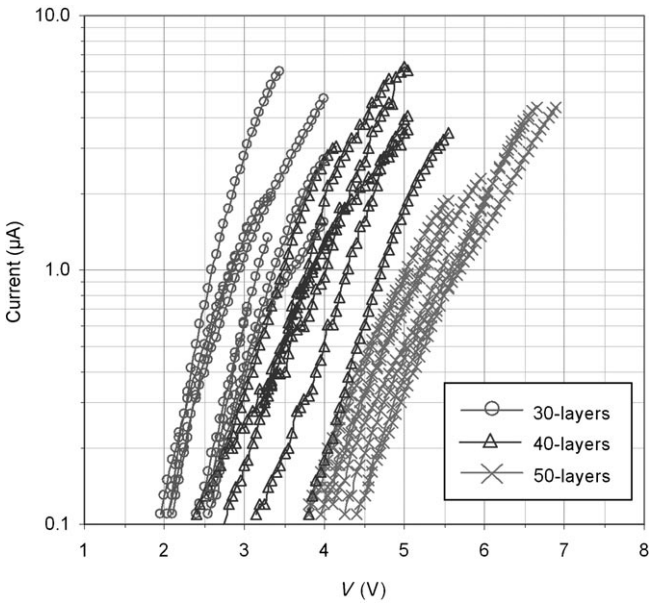

Figure 9. Current–voltage characteristics of 30, 40, and 50 bilayer CdTe/PDDA devices. The curves span regularly from lower to higher voltages in accordance with the number of layers; this suggests a field dependency of the current, as the number of layers determines the thickness *d* of the emissive layer and thus the electric field V/*d*. The small change in switch-on voltage for each subset of samples is attributed to variations at the multilayer–electrode interface. Reprinted from Ref. [57], Copyright 2007, with permission from the American Institute of Physics.

devices had an emissive area of 4 mm^2. The samples showed stable currents and the light output was recorded at operational current densities in the range of 100 $\mu A\,cm^{-2}$, two orders of magnitude lower than reported in Ref. [55]. The lower magnitudes and improved temporal stability of the currents are due to the improved uniformity and homogeneity of the nanoparticle multilayers. This contributes to the reduction of the leakage current through structural defects and pinholes in the film and to the stabilization of the device against localized high-field areas prone to electrical breakdowns.

The best efficiencies were recorded for the 30-bilayer devices. As the number of layers increases, higher voltages are required for light emission, lowering the efficiency. For the 30-bilayer devices (Figure 10), a maximum radiant power of

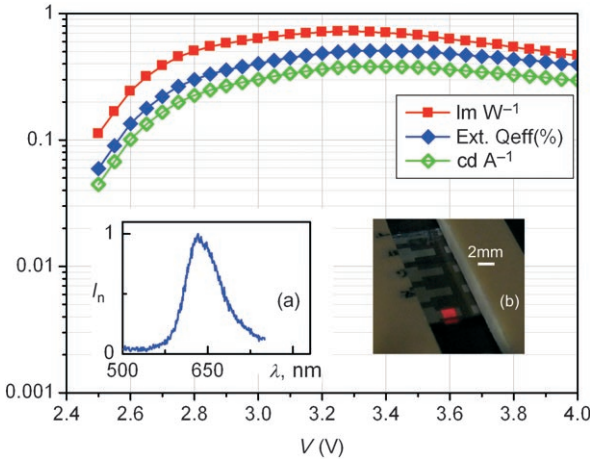

Figure 10. Efficiency values for the best performing 30-bilayer CdTe/PDDA device. The device showed an electroluminescence turn on at 2.5 V and the maximum light output was obtained at 3.3 V and 350 $mA\,cm^{-2}$, with a peak radiated power of 141 nW corresponding to an external quantum efficiency of 0.51 %. Taking into account the wavelength of emission (i.e. 630 nm), the luminous efficiencies reach 0.4 $cd\,A^{-1}$ and 0.81 $Lm\,W^{-1}$. The insets show a) the emission spectrum of a 30-bilayer device and b) a view of the emissive area while the device is operated in standard laboratory conditions without sealing or packaging. Reprinted from Ref. [57], Copyright 2007, with permission from the American Institute of Physics.

141 nW was measured at current densities of 350 $\mu A\,cm^{-2}$ ($I \approx 4.05\ \mu A$) and 3.3 V. The insets (a) and (b) in Figure 10 show the emission spectrum centered at 630 nm and a photograph of the device operating on a laboratory bench, emitting a clear red light. Assuming monochromatic emission, the maximum radiant power corresponds to an external quantum efficiency of 0.51 % and to luminous efficiencies of 0.8 $Lm\,W^{-1}$ (3.37×10^{-5} Lm) and 0.4 $cd\,A^{-1}$ (5.37×10^{-6} cd); the brightness peaks reaches it maximum at 1.42 $cd\,m^{-2}$. This value represents a fivefold improvement with respect to a similar device in Ref. [55].

It can be noted that the efficiencies and figures of merit from the devices that we tested are below that required for a commercial device. However, a review of other display technologies shows that, for example, the initial OLED devices were operating at 1.5 $Lm\,W^{-1}$ at an operating voltage of 10 V (original paper by Tang and Van Slyke).[58] These OLED type devices are now becoming a commercial reality and so it seems possible that with a similar development effort this new type of nanocrystal–LED device architecture could also become a niche commercial product.

4. Diffusion-Related Degradation Mechanisms in Semiconductor Nanocrystal LEDs

Gao et al.[53] have described damage in hybrid polymer/nanocrystal devices caused by the current-assisted oxidation of the aluminum cathode. In the case of OLEDs, the formation of dark spots has been related to the localized delamination of metallic cathodes, caused by electromigration at high operational fields.[59,60] Furthermore, Gautier et al.[61] found that field-induced damage to ITO electrodes can lead to device failure. Hirose et al.[62,63] reported the spontaneous diffusion of reactive metals such as indium and aluminum deposited on top of the organic layer. Schlatmann et al.[64] studied the diffusion of the underlying indium into organic layers in OLEDs prior to device operation. Chao et al.[65] explained the field-induced diffusion as a consequence of the decomposition of the ITO. We studied electrode-diffusion-related degradation mechanisms in nanocrystal/polymer composite LEDs of the sort described above.[66] The film thicknesses of the different materials are 35 nm, 220 nm, and 130 nm for aluminum, multilayer, and ITO, respectively. Each substrate had up to six identical independently addressable devices with an active area of 4 mm^2 (Figure 11). Four of these devices were biased at 4.0 V for 15 s, two under moderate vacuum (10^{-5} mbar), and the other two in air.

The electric field was approximately $1.8 \times 10^7\ V\,m^{-1}$ and measured currents were below 1 μA (25 $\mu A\,cm^{-2}$) in all cases,

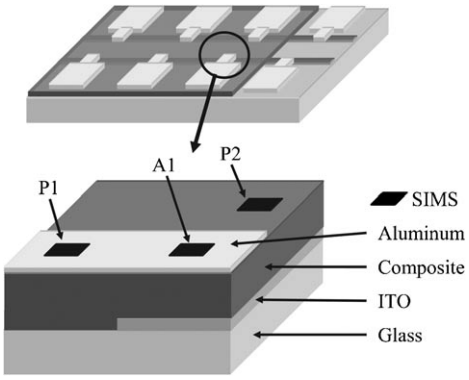

Figure 11. The structure of a device consisting of a composite CdTe/PDDA multilayer sandwiched between an aluminum cathode and an ITO anode. Device currents were 25 $\mu A\,cm^{-2}$ (maximum), with an applied bias of 4 V (or $10^7\ V\,m^{-1}$). The areas analyzed with SIMS are marked with black squares. The device's active area is that where cathode and anode cross (A1). Two different types of passive areas were studied: aluminum plus multilayer (P1), and multilayer plus ITO (P2). Reprinted from Ref. [66].

and dropped by 80–100% over the measurement period. Compositional depth profiles were acquired by secondary ion mass spectrometry (SIMS). The species examined were Al_{27}^+, In_{115}^+, and O_{16}^-. The composition profiles were taken in both active and passive areas. Active areas were those where the cathode and anode cross, and across which the field is applied.

The aluminum depth profiles for the areas A1 and P1 are shown in Figure 12. The vertical discontinuous lines are added

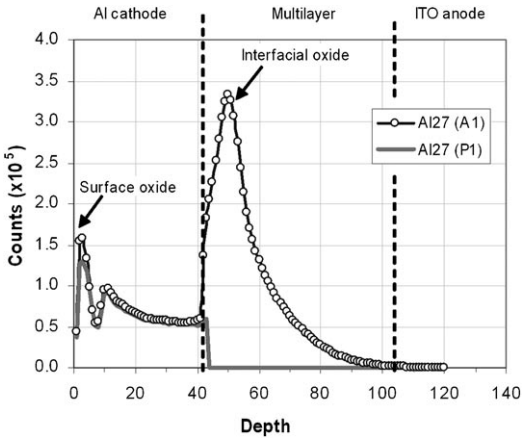

Figure 12. Aluminum depth profiles from areas A1 (circles) and P1 (line) of the device shown in Figure 11. The broken vertical lines mark the interfaces between the electrodes and the multilayer. The location of these interfaces is an indication only, derived from AFM and white light interferometry (WLI) measurements. Although the aluminum has been negatively biased, it can be seen that there is a significant diffusion of aluminum into the composite in area A1. This diffusion is caused by the strong applied field. Electromigration is ruled out because of the low current densities measured during the biasing of the devices. Reprinted from Ref. [66]

to indicate the boundary between organic and inorganic material. Both A1 and P1 areas showed an aluminum peak near the top surface of the sample. This small peak is associated with the passivating oxide film that forms on aluminum when exposed to the air. After this feature the intensity stabilized, with little variation between the readings from active and passive areas. It is reasonable to link this region to the "bulk" of the cathode film. After a small peak at the interface between the cathode and the organic multilayer, the aluminum intensity falls sharply in the passive area, and remains practically zero for the rest of the analysis. However, in the active area the aluminum intensity in fact increases at the interface with the multilayer and decreases gradually across the whole composite film. This profile is attributed to the diffusion of aluminum atoms during the biasing of the device. Any possible influence that pinhole formation during cathode deposition has on the aluminum distribution within the organic layer can be discarded because of the sharp aluminum edge in the depth profile shown by the adjacent P1 area (see Figure 11). It is important to remember that the variation in composition with sample depth results in different milling rates of the ion beam. Thus, the actual amplitude of the interfacial peak in the active areas following the cathode/multilayer interface must not be interpreted in terms of an aluminum abundance higher than in the bulk of the electrode (which would clearly be unreasonable), but as a change in the chemical nature of the materials present at that depth.

Figure 13 shows the oxygen profiles of the same areas A1 and P1 of Figure 12. Both profiles showed a first peak at the surface in contact with air, indicating the presence of a surface

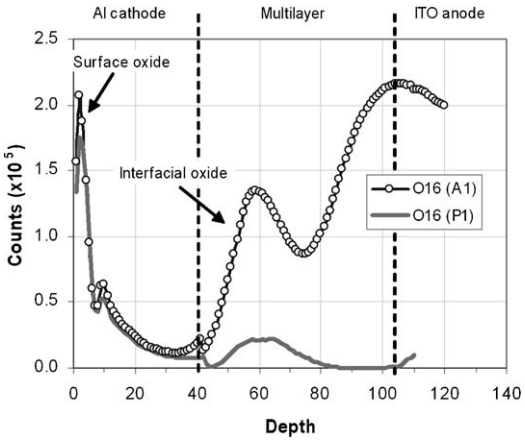

Figure 13. Oxygen depth profiles from the areas A1 and P1 as in Figure 12. The intensity of the peak beginning at the cathode/multilayer interface is substantially higher in the active area, denoting an extra content of oxygen at this region. This extra oxygen is associated with the oxidation of the diffused aluminum. The oxygen peak in A1 near the interface with the anode is due to the diffusion of oxygen from the ITO. Reprinted from Ref. [66].

oxide, as described above for aluminum. Both intensities then decayed smoothly with increasing depth into the cathode, showing similar intensities for both active and passive areas. As with aluminum, the differences between active and passive areas start at the interface between the cathode and the multilayer. The active area presented a clear second oxygen peak just after the interface; that peak was also present in the passive area P1, but the readings were around 85% lower than in the active area. The agreement in the data collected from the different devices indicates a homogeneous composition for active and passive areas before any of the devices were biased. We therefore conclude that the second peak in area A1 must have evolved while the device was biased. The evolution of this peak is associated with a change in chemical environment for the aluminum, indicating the presence of incorporated oxygen. The additional oxygen in area A1 is related to the oxidation of the diffused aluminum, as a result of oxygen absorption from the environment surrounding the device (at an environmental pressure of 10^{-5} mbar there should be enough oxygen present to oxidize the diffusing aluminum). This diffusion of environmental oxygen into polymeric layers during device operation has already been reported for other structures.[53,60] The active area also presented a third oxygen peak deeper into the organic layer that is absent from the profile of the P1 area. The peak, however, is present in the P2 area and is thus associated with the ITO anode.

The indium depth profile determined in the active area is shown in Figure 14 together with, for reference, that of oxygen. It can be seen that substantial indium contamination

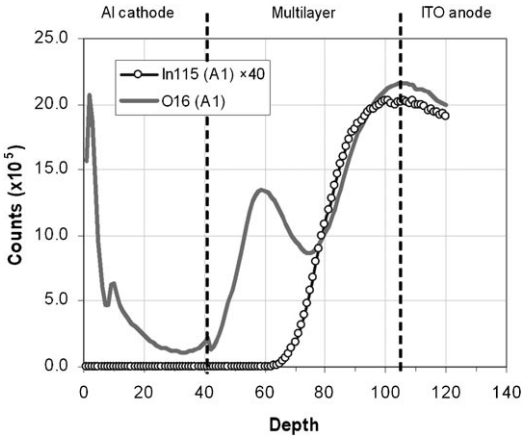

Figure 14. Indium and oxygen depth profiles from area A1. The indium has diffused over more than 65% of the multilayer thickness. The oxygen peak near the ITO anode matches the indium profile at that depth, indicating that O and In are associated with each other, that is, arise from the same source. Reprinted from Ref. [66].

is found in the organic multilayer. The indium penetration depth (corresponding to an indium count lower than 1% of the peak value) is approximately equivalent to 65% of the multilayer thickness. The shape of the indium profile matches the third oxygen peak, suggesting that this oxygen is associated with the diffused indium in the form of indium oxide. Indium diffusion into the organic multilayer can also be detected in area P2, with a penetration of 40% of the thickness of the multilayer. Indium diffusion is therefore present even in areas in which a field has not been applied—in contrast to the case of aluminum. The indium penetration is carried an additional 25% further into the composite on the application of an electric field.

It is concluded that the diffusion of metallic ions from the electrodes is a mechanism involved in the degradation of devices built with organic layers or composites. The diffusion of indium has previously been identified as a cause of defects that lead to device degradation. In this case a cathode diffusion mechanism resulting exclusively from the applied field was found which can induce structural defects even in low-current regimes. Field-driven aluminum diffusion and oxidation has been shown to produce an insulating barrier that reduces the conductivity of the device, causing irreversible device failure. Suitable cathodic diffusion barriers compatible with electron injection might result in an improvement of device lifetime and performance, both in OLED and hybrid organic-semiconductor–inorganic-nanoparticle systems.

5. Conclusions

Research on semiconductor nanocrystal-based LEDs has achieved a remarkable development in just one decade, resulting in more than two orders of magnitude improvement in the external quantum efficiency and providing highly saturated color emission. Although the device efficiencies are still over an order of magnitude lower than those of the purely organic counterparts, there are a number of potential advantages associated with nanocrystal-based devices, such as the possibility to achieve a spectrally pure emission color which will certainly merit future research. A variety of device configurations have become available including the promising sandwich architecture comprising only one monolayer of nanocrystals which serve exclusively as emitters. Further technological improvements of nanocrystal/organic LEDs aimed at optimizing charge injection and transport are bound to follow.

This work was supported by the EU project IST-2002-38195 FUNLIGHT "Functional Nanoscale Materials and Devices for Light Emission", by the EU NoE "PHOREMOST" "Nano-Photonics to Realise Molecular-Scale Technologies", and by the Deutsche Forschungsgemeinschaft (DFG).

Received: November 5, 2007
Published online: July 30, 2008

[1] *Organic Light-Emitting Devices* (Eds.: K. Müllen, U. Scherf), Wiley-VCH, Weinheim, **2006**.
[2] D. J. Milliron, I. Gur, A. P. Alivisatos, *MRS Bull.* **2005**, *30*, 41.
[3] Al. L. Efros, A. L. Efros, *Sov. Phys. Semicond.* **1982**, *16*, 772.
[4] C. B. Murray, D. J. Norris, M. G. Bawendi, *J. Am. Chem. Soc.* **1993**, *115*, 8706.
[5] N. Gaponik, D. V. Talapin, A. L. Rogach, K. Hoppe, E. V. Shevchenko, A. Kornowski, A. Eychmüller, H. Weller, *J. Phys. Chem. B* **2002**, *106*, 7177.
[6] A. L. Rogach, A. Eychmüller, S. G. Hickey, S. V. Kershaw, *Small* **2007**, *3*, 536.
[7] S. J. Rosenthal, J. McBride, S. J. Pennycook, L. C. Feldman, *Surf. Sci. Rep.* **2007**, *62*, 111.
[8] C. de Mello Donega, P. Liljeroth, D. Vanmaekelbergh, *Small* **2005**, *1*, 1152.
[9] A. L. Rogach, T. Franzl, T. A. Klar, J. Feldmann, N. Gaponik, V. Lesnyak, A. Shavel, A. Eychmüller, Y. P. Rakovich, J. F. Donegan, *J. Phys. Chem. C* **2007**, *111*, 14628.
[10] C. B. Murray, C. R. Kagan, M. G. Bawendi, *Annu. Rev. Mater. Sci.* **2000**, *30*, 545.
[11] A. L. Rogach, D. V. Talapin, E. V. Shevchenko, A. Kornowski, M. Haase, H. Weller, *Adv. Funct. Mater.* **2002**, *12*, 653.
[12] B. O. Dabbousi, J. Rodriguez-Viejo, F. V. Mikulec, J. R. Heine, H. Mattoussi, R. Ober, K. F. Jensen, M. G. Bawendi, *J. Phys. Chem. B* **1997**, *101*, 9463.
[13] X. Peng, M. C. Schlamp, A. V. Kadavanich, A. P. Alivisatos, *J. Am. Chem. Soc.* **1997**, *119*, 7019.
[14] E. Holder, N. Tessler, A. Rogach, *J. Mater. Chem.* **2008**, *18*, 1064.
[15] C. A. Leatherdale, C. R. Kagan, N. Y. Morgan, S. A. Empedocles, M. A. Kastner, M. G. Bawendi, *Phys. Rev. B* **2000**, *62*, 2669.
[16] M. Drndic, M. V. Jarosz, N. Y. Morgan, M. A. Kastner, M. G. Bawendi, *J. Appl. Phys.* **2002**, *92*, 7498.
[17] D. S. Ginger, N. C. Greenham, *J. Appl. Phys.* **2000**, *87*, 1361.
[18] V. L. Colvin, M. C. Schlamp, A. P. Alivisatos, *Nature* **1994**, *370*, 354.
[19] B. O. Dabbousi, M. G. Bawendi, O. Onitsuka, M. F. Rubner, *Appl. Phys. Lett.* **1995**, *66*, 1316.
[20] M. C. Schlamp, X. Peng, A. P. Alivisatos, *J. Appl. Phys.* **1997**, *82*, 5837.

[21] H. Mattoussi, L. H. Radzilowski, B. O. Dabbousi, E. L. Thomas, M. G. Bawendi, M. F. Rubner, *J. Appl. Phys.* **1998**, *83*, 7965.
[22] Y. Yang, S. Xue, S. Liu, J. Huang, J. Shen, *Appl. Phys. Lett.* **1996**, *69*, 377.
[23] H. Yang, P. H. Holloway, B. B. Ratna, *J. Appl. Phys.* **2003**, *93*, 586.
[24] J. Zhao, J. Zhang, C. Jiang, J. Bohnenberger, T. Basche, A. Mews, *J. Appl. Phys.* **2004**, *96*, 3206.
[25] R. A. M. Hikmet, D. V. Talapin, H. Weller, *J. Appl. Phys.* **2003**, *93*, 3509.
[26] R. A. M. Hikmet, P. T. K. Chin, D. V. Talapin, H. Weller, *Adv. Mater.* **2005**, *17*, 1436.
[27] A. H. Mueller, M. A. Petruska, M. Achermann, D. J. Werder, E. A. Akhadov, D. D. Koleske, M. A. Hoffbauer, V. I. Klimov, *Nano Lett.* **2005**, *5*, 1039.
[28] M. Achermann, M. A. Petruska, D. D. Koleske, M. H. Crawford, V. I. Klimov, *Nano Lett.* **2006**, *6*, 1396.
[29] J. Zhao, J. A. Bardecker, A. M. Munro, M. S. Liu, Y. Niu, I.-K. Ding, J. Luo, B. Chen, A. K.-Y. Jen, D. S. Ginger, *Nano Lett.* **2006**, *6*, 463.
[30] Y. H. Niu, A. M. Munro, Y. J. Cheng, Y. Q. Tian, M. S. Liu, J. L. Zhao, J. A. Bardecker, I. Jen-La Plante, D. S. Ginger, A. K.-Y. Jen, *Adv. Mater.* **2007**, *19*, 3371.
[31] Q. Sun, Y. A. Wang, L. S. Li, D. Wang, T. Zhu, J. Xu, C. Yang, Y. Li, *Nat. Photonics* **2007**, *1*, 717.
[32] S. Coe, W.-K. Woo, M. Bawendi, V. Bulovic, *Nature* **2002**, *420*, 800.
[33] S. Coe-Sullivan, W.-K. Woo, J. S. Steckel, M. Bawendi, V. Bulovic, *Org. Electron.* **2003**, *4*, 123.
[34] J. S. Steckel, P. Snee, S. Coe-Sullivan, Z. J. P. , J. E. Halpert, P. Anikeeva, L.-A. Kim, V. Bulovic, M. G. Bawendi, *Angew. Chem.* **2006**, *118*, 5928; *Angew. Chem. Int. Ed.* **2006**, *45*, 5796.
[35] S. Chaudhary, M. Ozkan, W. C. W. Chan, *Appl. Phys. Lett.* **2004**, *84*, 2925.
[36] Y. Q. Li, A. Rizzo, R. Cingolani, G. Gigli, *Microchim. Acta* **2007**, *159*, 207.
[37] Y. Li, A. Rizzo, M. Mazzeo, L. Carbone, L. Manna, R. Cingolani, G. Gigli, *J. Appl. Phys.* **2005**, *97*, 113501.
[38] P. O. Anikeeva, J. E. Halpert, M. G. Bawendi, V. Bulovic, *Nano Lett.* **2007**, *7*, 2196.
[39] J. H. Ahn, C. Bertoni, S. Dunn, C. Wang, D. V. Talapin, N. Gaponik, A. Eychmüller, Y. Hua, M. R. Bryce, M. C. Petty, *Nanotechnology* **2007**, *18*, 335202/1.
[40] K. T. Kamtekar, C. Wang, S. Bettington, A. S. Batsanov, I. F. Perepichka, M. R. Bryce, J. H. Ahn, M. Rabinal, M. C. Petty, *J. Mater. Chem.* **2006**, *16*, 3823.
[41] J. H. Park, J. Y. Kim, B. D. Chin, Y. C. Kim, J. K. Kim, O. O. Park, *Nanotechnology* **2004**, *15*, 1217.
[42] A. R. Duggal, J. J. Shiang, C. M. Heller, D. F. Foust, *Appl. Phys. Lett.* **2002**, *80*, 3470.
[43] A. Shavel, N. Gaponik, A. Eychmüller, *J. Phys. Chem. B* **2004**, *108*, 5905.
[44] A. Shavel, N. Gaponik, A. Eychmüller, *J. Phys. Chem. B* **2006**, *110*, 19280.
[45] A. L. Rogach, T. Franzl, T. A. Klar, J. Feldmann, N. Gaponik, V. Lesnyak, A. Shavel, A. Eychmüller, Y. P. Rakovich, J. F. Donegan, *J. Phys. Chem. C* **2007**, *111*, 14628.
[46] A. L. Rogach, M. T. Harrison, S. V. Kershaw, A. Kornowski, M. G. Burt, A. Eychmüller, H. Weller, *Phys. Status Solidi B* **2001**, *224*, 153.
[47] N. P. Gaponik, D. V. Talapin, A. L. Rogach, *Phys. Chem. Chem. Phys.* **1999**, *1*, 1787.
[48] N. P. Gaponik, D. V. Talapin, A. L. Rogach, A. Eychmüller, *J. Mater. Chem.* **2000**, *10*, 2163.
[49] G. Decher, *Science* **1997**, *277*, 1232.
[50] J. H. Cheng, A. F. Fou, M. F. Rubner, *Thin Solid Films* **1994**, *244*, 985.
[51] A. L. Rogach, D. S. Koktysh, M. Harrison, N. A. Kotov, *Chem. Mater.* **2000**, *12*, 1526.
[52] M. Gao, B. Richter, S. Kirstein, *Adv. Mater.* **1997**, *9*, 802.
[53] M. Gao, B. Richter, S. Kirstein, H. Möhwald, *J. Phys. Chem. B* **1998**, *102*, 4096.
[54] J. Müller, J. M. Lupton, A. L. Rogach, J. Feldmann, D. V. Talapin, H. Weller, *Appl. Phys. Lett.* **2004**, *85*, 381.
[55] M. Gao, C. Lesser, S. Kirstein, H. Möhwald, A. L. Rogach, H. Weller, *J. Appl. Phys.* **2000**, *87*, 2297.
[56] W. Chen, D. Grouquist, J. Roark, *J. Nanosci. Nanotechnol.* **2002**, *2*, 47.
[57] C. Bertoni, D. Gallardo, S. Dunn, N. Gaponik, A. Eychmüller, *Appl. Phys. Lett.* **2007**, *90*, 034107.
[58] C. W. Tang, S. A. VanSlyke, *Appl. Phys. Lett.* **1987**, *51*, 913.
[59] B. H. Cumpston, K. F. Jensen, *Appl. Phys. Lett.* **1996**, *69*, 3941.
[60] B. H. Cumpston, I. D. Parker, K. F. Jensen, *J. Appl. Phys.* **1997**, *81*, 3716.
[61] E. Gautier, A. Lorin, J.-M. Nunzi, A. Schalchli, J.-J. Benattar, D. Vital, *Appl. Phys. Lett.* **1996**, *69*, 1071.
[62] Y. Hirose, A. Kahn, V. Aristov, P. Soukiassian, V. Bulovic, S. R. Forrest, *Phys. Rev. B* **1996**, *54*, 13748.
[63] Y. Hirose, A. Kahn, V. Aristov, P. Soukiassian, *Appl. Phys. Lett.* **1996**, *68*, 217.
[64] A. R. Schlatmann, D. W. Floet, A. Hilberer, F. Garten, P. J. M. Smuldars, T. M. Klapwijk, G. Hadziioannou, *Appl. Phys. Lett.* **1996**, *69*, 1764.
[65] C. I. Chao, K. R. Chuang, S. A. Chen, *Appl. Phys. Lett.* **1996**, *69*, 2894.
[66] D. E. Gallardo, C. Bertoni, S. Dunn, N. Gaponik, A. Eychmüller, *Adv. Mater.* **2007**, *19*, 3364.